



# Update on NREL's 2020 Offshore Wind Resource Assessment for the California Pacific Outer Continental Shelf

Nicola Bodini,<sup>1</sup> Alex Rybchuk,<sup>1</sup> Mike Optis,<sup>2</sup> Walter Musial,<sup>1</sup> Julie K. Lundquist,<sup>1,3,4</sup> Stephanie Redfern,<sup>1</sup> Caroline Draxl,<sup>1,4</sup> Raghavendra Krishnamurthy,<sup>5</sup> and Brian Gaudet<sup>5</sup>

*1 National Renewable Energy Laboratory (NREL)*

*2 Veer Renewables Inc.*

*3 Department of Atmospheric and Oceanic Sciences, University of Colorado Boulder*

*4 Renewable and Sustainable Energy Institute, University of Colorado, Boulder*

*5 Pacific Northwest National Laboratory*

*Produced under direction of the Bureau of Ocean Energy Management (BOEM) by the National Renewable Energy Laboratory under Interagency Agreement IAG-19-02123-4.*

**NREL is a national laboratory of the U.S. Department of Energy  
Office of Energy Efficiency & Renewable Energy  
Operated by the Alliance for Sustainable Energy, LLC**

This report is available at no cost from the National Renewable Energy Laboratory (NREL) at [www.nrel.gov/publications](http://www.nrel.gov/publications).

Contract No. DE-AC36-08GO28308

**Strategic Partnership Project Report**  
NREL/TP-5000-83756  
OCS Study BOEM 2022-072  
November 2022



# Update on NREL's 2020 Offshore Wind Resource Assessment for the California Pacific Outer Continental Shelf

Nicola Bodini,<sup>1</sup> Alex Rybchuk,<sup>1</sup> Mike Optis,<sup>2</sup> Walter Musial,<sup>1</sup> Julie K. Lundquist,<sup>1,3,4</sup> Stephanie Redfern,<sup>1</sup> Caroline Draxl,<sup>1,4</sup> Raghavendra Krishnamurthy,<sup>5</sup> and Brian Gaudet<sup>5</sup>

*1 National Renewable Energy Laboratory (NREL)*

*2 Veer Renewables Inc.*

*3 Department of Atmospheric and Oceanic Sciences, University of Colorado Boulder*

*4 Renewable and Sustainable Energy Institute, University of Colorado, Boulder*

*5 Pacific Northwest National Laboratory*

## Suggested Citation

Bodini, Nicola, Alex Rybchuk, Mike Optis, Walter Musial, Julie K. Lundquist, Stephanie Redfern, Caroline Draxl, Raghavendra Krishnamurthy, and Brian Gaudet. 2022. *Update on NREL's 2020 Offshore Wind Resource Assessment for the California Pacific Outer Continental Shelf*. Golden, CO: National Renewable Energy Laboratory. NREL/TP-5000-83756. <https://www.nrel.gov/docs/fy23osti/83756.pdf>.

**NREL is a national laboratory of the U.S. Department of Energy  
Office of Energy Efficiency & Renewable Energy  
Operated by the Alliance for Sustainable Energy, LLC**

This report is available at no cost from the National Renewable Energy Laboratory (NREL) at [www.nrel.gov/publications](http://www.nrel.gov/publications).

Contract No. DE-AC36-08GO28308

**Strategic Partnership Project Report**  
NREL/TP-5000-83756  
OCS Study BOEM 2022-072  
November 2022

National Renewable Energy Laboratory  
15013 Denver West Parkway  
Golden, CO 80401  
303-275-3000 • [www.nrel.gov](http://www.nrel.gov)

## NOTICE

This work was authored in part by the National Renewable Energy Laboratory, operated by Alliance for Sustainable Energy, LLC, for the U.S. Department of Energy (DOE) under Contract No. DE-AC36-08GO28308. Funding provided by the U.S. Department of Energy Office of Energy Efficiency and Renewable Energy Wind Energy Technologies Office, by the Bureau of Ocean Energy Management under agreement number IAG-19-2123-4, and by the National Offshore Wind Research and Development Consortium under agreement no. CRD-19-16351. The Pacific Northwest National Laboratory is operated by Battelle Memorial Institute for DOE under Contract DE-AC05-76RL01830. The views expressed herein do not necessarily represent the views of the DOE or the U.S. Government.

This report is available at no cost from the National Renewable Energy Laboratory (NREL) at [www.nrel.gov/publications](http://www.nrel.gov/publications).

U.S. Department of Energy (DOE) reports produced after 1991 and a growing number of pre-1991 documents are available free via [www.OSTI.gov](http://www.OSTI.gov).

*Cover Photos by Dennis Schroeder: (clockwise, left to right) NREL 51934, NREL 45897, NREL 42160, NREL 45891, NREL 48097, NREL 46526.*

NREL prints on paper that contains recycled content.

## List of Acronyms

cRMSE	centered (unbiased) root-mean-square error
CA20	20-year wind resource data set produced in 2020 by NREL for the California OCS
GCF	gross capacity factor
km	kilometer
LSM	land-surface model
m	meter
MCP	measure-correlate-predict
MYNN	Mellor-Yamada-Nakanishi-Niino
NREL	National Renewable Energy Laboratory
OCS	Outer Continental Shelf
PBL	planetary boundary layer
PNNL	Pacific Northwest National Laboratory
SST	sea-surface temperature
WRF	Weather Research and Forecasting (model)
YSU	Yonsei University

## Executive Summary

This report provides a time-sensitive update to the 20-year wind resource data set (named “CA20”) produced in 2020 by the National Renewable Energy Laboratory (NREL) for the Outer Continental Shelf off the coast of California. The findings in this report represent the best information available as of August 31, 2022.

Following the deployment of two floating lidars in the region in late 2020, NREL compared the CA20-modeled wind speeds against the lidar measurements using two different approaches:

1. Comparison of lidar observations against a 1-year extension of the CA20 data set that overlapped with the lidar period of record (October 2020–September 2021).
2. Comparison of the original 20-year CA20 data set against a synthetic, long-term-adjusted lidar data set that matched the CA20 period of record (2000–2019), which was obtained by applying the measure-correlate-predict method to the short-term lidar observations and the ERA-5 reanalysis product.

The two validation approaches yielded different results. The first approach showed average biases in the 150-meter (m) modeled wind speeds of around  $1.8 \text{ m s}^{-1}$  at Humboldt and  $0.7 \text{ m s}^{-1}$  at Morro Bay (Figure ES-1), with little diurnal or annual variability.

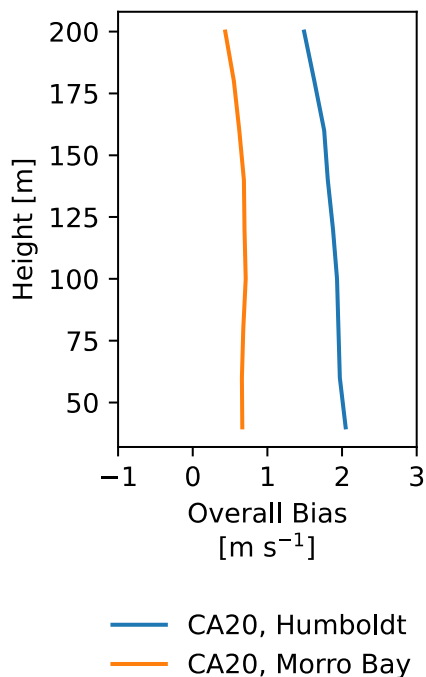


**Figure ES-1. Vertical profiles of mean bias between the 1-year CA20 extension and concurrent, short-term floating lidar observations at Humboldt and Morro Bay**

However, the lidar period of record at Humboldt was only 7 months, was seasonally biased, and had highly anomalous wind conditions. Therefore, biased results found in this short-term validation are not necessarily fully representative of the long-term CA20 performance. The second validation approach considered the full 20-year period of the CA20 simulations, with the caveat that CA20 can only be evaluated against a synthetic lidar data set over such period. The results from this second validation approach showed average biases of 1.3 m s<sup>-1</sup> at Humboldt and 1.0 m s<sup>-1</sup> at Morro Bay for 150-m wind speeds (Table ES-1).

**Table ES-1. Comparison of Mean Wind Speeds and Gross Capacity Factor Values Derived from the CA20 and Synthetic Long-Term-Adjusted Lidar Data Sets**

Site	Mean 150-m Wind Speed (meters per second [m/s])		Gross Capacity Factor (%)	
	Synthetic Long-Term-Adjusted Lidar	CA20	Synthetic Long-Term-Adjusted Lidar	CA20
Humboldt	9.3	10.6	55.6	58.6
Morro Bay	9.0	10.0	54.6	57.2

Next, we investigated the impact of these wind speed biases on gross energy estimates. Using the 20-year time series for both CA20 and the synthetic long-term-adjusted lidar data—extracted at the lidar locations—we calculated gross capacity factors for a single International Energy Agency Wind 15-megawatt turbine. As shown in Table ES-1, gross capacity factors were found to be about 3 percentage points higher when using CA20 compared to the synthetic long-term-adjusted lidar data. This limited energy bias occurred because most of the extreme CA20 wind speed biases were found in high wind speed regimes where turbines would already be operating at rated power. In the more critical 3–10 m s<sup>-1</sup> wind speed range, where wind speed biases would be most impactful on produced energy, the CA20 bias was lower.

Further research began in summer 2022 to better understand the reasons behind the CA20 bias. Preliminary analysis suggests that the choice of the planetary boundary layer scheme within the numerical model could be connected to a large portion of the observed bias, with the Yonsei University planetary boundary layer scheme providing a better match with the lidar observations than the Mellor-Yamada-Nakanishi-Niino scheme used in CA20. This more in-depth analysis is expected to identify the physical drivers of the observed bias. The results of this analysis will be published by NREL and the Pacific Northwest National Laboratory in due course, together with a revised CA20 data set. In the meantime, NREL recommends caution when using CA20 for detailed energy analyses (e.g., seasonal and diurnal trends). CA20 users should fully consider the results of the bias identified herein and be aware that the sources of bias are still being investigated and will be better understood and described in future reports.

# Table of Contents

List of Acronyms.....	iv
Executive Summary.....	v
List of Figures.....	vii
List of Tables.....	viii
<b>1 Introduction.....</b>	<b>1</b>
<b>2 Data and Methods.....</b>	<b>2</b>
2.1 Lidar Observations.....	2
2.2 Weather Research and Forecasting Simulation.....	3
2.3 Short-Term Validation Approach.....	4
2.4 Long-Term Adjusted Validation Approach.....	4
<b>3 Short-Term Validation Results.....</b>	<b>6</b>
3.1 Short-Term Wind Speed Bias as a Function of Wind Speed.....	7
3.2 Temporal Variability of Short-Term Wind Speed Bias.....	7
3.3 Distributions of Wind Speed, Wind Direction, and Shear.....	8
<b>4 Long-Term Validation Results.....</b>	<b>10</b>
4.1 Lidar Period of Record Anomalies.....	10
4.2 A Long-Term Validation Approach.....	11
4.3 Impact On Long-Term Energy.....	12
<b>5 Impact of the Choice of the Planetary Boundary Layer Scheme.....</b>	<b>14</b>
<b>6 Conclusions and Next Steps.....</b>	<b>16</b>
References.....	17

## List of Figures

Figure ES-1. Vertical profiles of mean bias between the 1-year CA20 extension and concurrent, short-term floating lidar observations at Humboldt and Morro Bay.....	v
Figure 1. Locations of the two floating lidars in the California OCS. The grey areas show the current Bureau of Ocean Energy Management Call Areas in the region. ....	2
Figure 2. Percent lidar data availability by month.....	3
Figure 3. (a) Bias, (b) cRMSE, and (c) R <sup>2</sup> calculated at Humboldt and Morro Bay for the WRF validation run compared to the floating lidar observations.....	6
Figure 4. The 120-m wind speed bias as a function of observed wind speed at (a) Humboldt and (b) Morro Bay. The number of hourly average observations in each wind speed bin (left y-axis) is overlaid as a bar plot. ....	7
Figure 5. The 120-m average wind speed as a function of hour at (a) Humboldt and (c) Morro Bay. Similarly, the 120-m average wind speed as a function of month at (b) Humboldt and (d) Morro Bay. Local time (Pacific Standard Time) may be found by subtracting 8 hours from the UTC time used in the plots.....	7
Figure 6. Distributions of 120-m wind speed, 120-m wind direction, and the shear parameter calculated between 40 m and 200 m at (left) Humboldt and (right) Morro Bay.....	9
Figure 7. Boxplots of the 20-year CA20 150-m monthly average wind speeds by calendar months at Humboldt (a) and Morro Bay (b). Black diamonds denote CA20 outliers. Red crosses denote the modeled mean monthly winds from the 1-year extension of CA20 over the lidar periods of record. ....	11
Figure 8. Scatterplots of hourly 100-m ERA5 and 150-m lidar wind speeds at (a) Humboldt and (b) Morro Bay. The square of the correlation coefficient and number of data points are also shown.....	12
Figure 9. Mean biases of hourly CA20 150-m wind speeds relative to synthetic long-term-adjusted lidar 150-m wind speeds for (a) Humboldt and (b) Morro Bay. Data are binned based on hourly synthetic long-term lidar wind speeds. Data counts for each bin are also shown. ....	13

Figure 10. (a) Bias, (b) cRMSE, and (c) R<sup>2</sup> calculated at Humboldt and Morro Bay for the WRF validation run using the YSU planetary boundary layer scheme, compared to the floating lidar observations..... 14

Figure 11. Distributions of 120-m wind speed, 120-m wind direction, and the shear parameter calculated between 40 m and 200 m at (left) Humboldt and (right) Morro Bay. Results shown in the figure are for the WRF simulation that uses the YSU PBL scheme. .... 15

## List of Tables

Table ES-1. Comparison of Mean Wind Speeds and Gross Capacity Factor Values Derived from the CA20 and Synthetic Long-Term-Adjusted Lidar Data Sets ..... vi

Table 1. Attributes of the 1-Year WRF Simulation Used in This Analysis, With the Same Setup as the 20-Year CA20 Data Set..... 4

Table 2. Mean 150-m Wind Speeds From the 20-year CA20 and Its 1-Year Extension..... 10

Table 3. Comparison of Mean 150-m Wind Speeds From Synthetic Long-Term-Corrected Lidar Data Set and CA20..... 12

Table 4. Comparison of GCF Values Derived From the CA20 and Synthetic Long-Term-Adjusted Lidar Data Sets..... 13

# 1 Introduction

In 2020, the National Renewable Energy Laboratory (NREL) produced and published a 20-year offshore wind resource assessment for the California Pacific Outer Continental Shelf (OCS) (Optis et al. 2020), named “CA20.” The data set was produced using the state-of-the-art Weather Research and Forecasting (WRF) model, with a specific model setup that was chosen after a validation against the observations collected in the region by an array of near-surface buoys and coastal radars, as well as observations from two floating lidars in the mid-Atlantic region. Specifically, the reanalysis-forcing product, the planetary boundary layer (PBL) scheme, the sea-surface temperature (SST) product, and the land-surface model (LSM) to use in the full 20-year WRF run were all selected based on the results of this validation.

As stated in Optis et al. (2020), all the measurements used for the model validation that were available at the time were insufficient to confirm the accuracy of model data. The buoys only have measurements close to the surface and, therefore, do not provide information on the wind resource at the heights relevant for wind energy purposes. The coastal radars provide measurements at more relevant heights but at the interface between the land and the ocean, where the model validation becomes uncertain because of large gradients of meteorological variables. Finally, the floating lidars in the mid-Atlantic domain provide ideal measurements for validating hub-height wind speeds, but in a completely different region, where domain-specific processes and features might determine a different optimal WRF setup than what is needed for the California OCS. The lack of floating lidar observations in the California OCS was recognized at the time as a significant limitation to the analysis and initial validation of CA20.

Subsequently, two floating lidars were deployed in the region. The comparison of CA20 with the lidar observations revealed a significant bias in the modeled data. This report describes this bias and its impact on energy assessments in the California OCS.

## 2 Data and Methods

### 2.1 Lidar Observations

In 2020, the Pacific Northwest National Laboratory (PNNL) deployed two floating lidars in the California OCS, near the Bureau of Ocean Energy Management Call Areas of Humboldt and Morro Bay (Figure 1). Observations from both lidars are publicly available (Atmosphere to Electrons 2021, 2022).

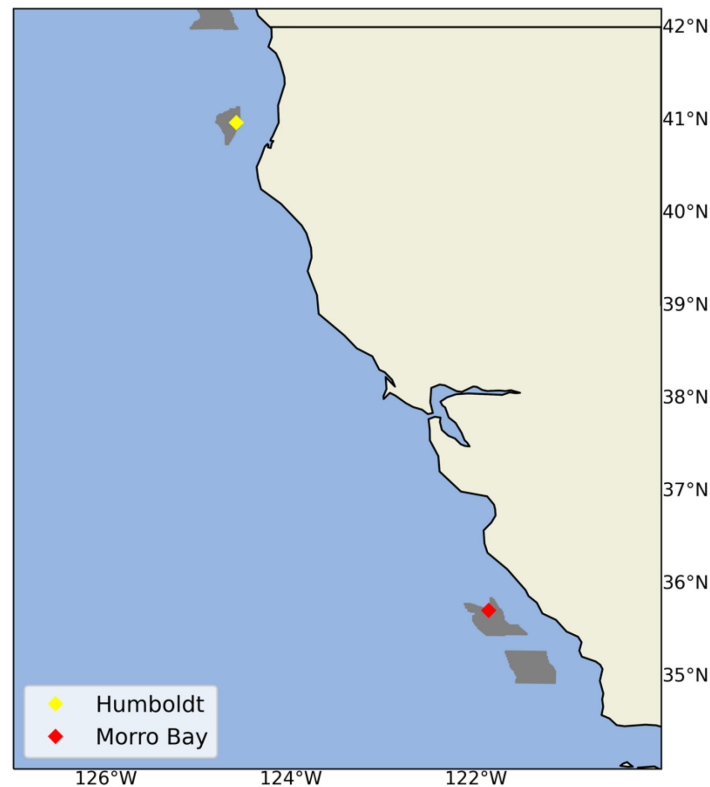


**Figure 1. Locations of the two floating lidars in the California OCS. The grey areas show the current Bureau of Ocean Energy Management Call Areas in the region.**

Both lidars started recording observations in October 2020. The Humboldt unit experienced a technical issue and had to be rescued, serviced, and redeployed, so observations at Humboldt are not available from January 2021 to late May 2021. The Humboldt buoy was recommissioned in May 2021 and has now collected data through June 2022; however, in our analysis, we only included observations until the end of September 2021 because of both a potential issue (under investigation by the instrument mentors at the time of writing) with the lidar observations starting in December 2021 and limited computing time available to run WRF. Lidar observations are available every 20 meters (m), from 40 to 200 m above the surface.

We filtered out lidar observations where the lidar data availability parameter (the percentage of valid wind estimations obtained over a given period of time and reported in the lidar data files) was lower than 80% (an arbitrary threshold that was agreed upon with the lidar instrument mentors), and all data points were internally flagged by the quality checks of the instrument. We

then calculated hourly average data to use for the WRF validation analysis. Figure 2 shows the resulting data availability for the two units throughout the 12 months considered in this report. Overall, we have 94.2% annual coverage at Morro Bay and 52.2% annual coverage at Humboldt (including the outage periods).

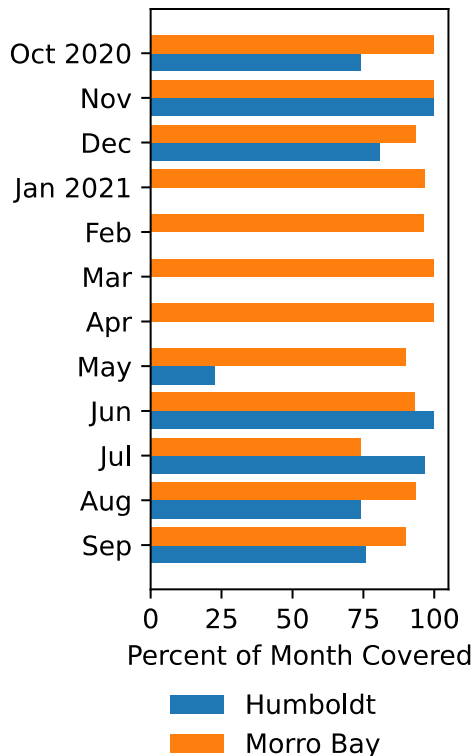


**Figure 2. Percent lidar data availability by month**

## 2.2 Weather Research and Forecasting Simulation

The CA20 WRF data set published by NREL covers the period from 2000–2019 and, therefore, does not overlap with the period of record of the two floating lidars in the region. To directly validate the WRF setup used for CA20, we extended the CA20 data set by running a yearlong WRF simulation (using the same setup used in CA20) to cover the period between October 2020 and September 2021. The WRF simulation was run using the same process and attributes described in the original CA20 report. Table 1 summarizes the main attributes of the WRF setup.

**Table 1. Attributes of the 1-Year WRF Simulation Used in This Analysis, With the Same Setup as the 20-Year CA20 Data Set**

Feature	Specification
<b>WRF version</b>	4.1.2
<b>Nesting</b>	6 kilometers (km), 2 km
<b>Vertical levels</b>	61
<b>Near-surface-level heights (meters)</b>	12, 34, 52, 69, 86, 107, 134, 165, 200
<b>Forcing</b>	ERA5
<b>Planetary boundary layer scheme</b>	Mellor-Yamada-Nakanishi-Niino
<b>Sea-surface temperature product</b>	Operational Sea Surface Temperature and Sea Ice Analysis (OSTIA)
<b>Land-surface model</b>	Noah
<b>Atmospheric nudging</b>	Spectral nudging on a 6-km domain, applied every 6 hours
<b>Microphysics</b>	Ferrier
<b>Longwave radiation</b>	Rapid Radiative Transfer Model
<b>Shortwave radiation</b>	Rapid Radiative Transfer Model
<b>Topographic database</b>	Global Multi-Resolution Terrain Elevation Data from the U.S. Geological Service and National Geospatial-Intelligence Agency
<b>Land-use data</b>	Moderate Resolution Imaging Spectroradiometer 30 seconds (s)
<b>Cumulus parameterization</b>	Kain-Fritsch

We then calculated the hourly averaged WRF-modeled wind resource from the grid cell nearest the lidar sites and used these data for the validation against the lidar observations.

### 2.3 Short-Term Validation Approach

The most straightforward validation approach was to compare the 1-year extension of the CA20 data set directly with the concurrent lidar measurements. To this end, we considered three validation metrics:

1. Bias
2. Centered (unbiased) root-mean-squared error (cRMSE)
3. Coefficient of determination ( $R^2$ ) (i.e., the square of the Pearson’s correlation coefficient)

We performed the validation at all the heights where lidar observations were available. WRF output data were linearly interpolated to these heights from the neighboring model levels. Given the high vertical resolution used in the model in the lowest 200 m, using a simple linear interpolation was a reasonable choice to approximate the vertical variability of wind over such short distances (Optis et al. 2020).

### 2.4 Long-Term Adjusted Validation Approach

The short period of record of the lidar observations at Humboldt risks leading to validation results that do not represent the long-term CA20 performance. To assess this risk, we applied the measure-correlate-predict (MCP) method (Brower 2012) on the short-term lidar observations and

the ERA-5 reanalysis product (Hersbach et al. 2020) to produce a 20-year synthetic lidar data set. Details of this method are provided in Section 4.2. We then assessed the bias of the full 20-year CA20 hourly winds compared to the synthetic long-term-corrected lidar time series data.

Validation results for the direct lidar validation are provided in Section 3, and results for the synthetic long-term-corrected lidar data are provided in Section 4.

### 3 Short-Term Validation Results

The overall results of the short-term comparison between the 1-year extended CA20 WRF run and the lidar observations are shown in Figure 3.

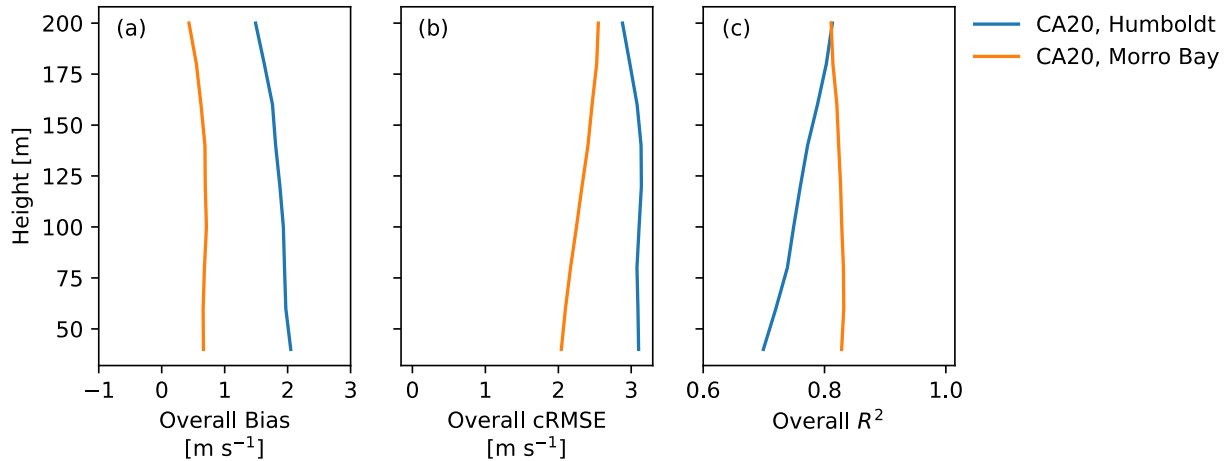


**Figure 3. (a) Bias, (b) cRMSE, and (c) R<sup>2</sup> calculated at Humboldt and Morro Bay for the WRF validation run compared to the floating lidar observations**

We found that the WRF model showed a large wind speed bias of approximately  $+2.0 \text{ m s}^{-1}$  at 40 m above the surface at Humboldt, which progressively decreased to about  $+1.5 \text{ m s}^{-1}$  at 200 m above the surface. At Morro Bay, the model showed a smaller magnitude bias of approximately  $+0.7 \text{ m s}^{-1}$  closer to the surface that dropped to about  $+0.45 \text{ m s}^{-1}$  at 200 m above the surface. When looking at cRMSE, the WRF showed a large cRMSE between 2.9 and 3.2  $\text{m s}^{-1}$  at Humboldt, whereas at Morro Bay, the cRMSE was between 2.0 and 2.5  $\text{m s}^{-1}$ , with a constant increase with height. The R<sup>2</sup> was larger at Morro Bay where it was nearly constant with height at around 0.82. At Humboldt, we found an increase of the R<sup>2</sup> with height, from 0.70 to 0.81.

The large bias of WRF at Humboldt exceeded the bias observed in other offshore WRF validation studies. For example, Pronk et al. (2022) compared WRF simulations with an identical configuration to the CA20 WRF runs to measurements from two floating lidars off the U.S. East Coast. They found that WRF had an approximately  $-0.5 \text{ m s}^{-1}$  bias at both lidars at all heights. The large WRF bias at Humboldt also significantly exceeded the bias observed across many locations by European colleagues that built the New European Wind Atlas. Hahmann et al. (2020) ran several yearlong sensitivity simulations to inform modeling decisions for the production New European Wind Atlas run, and they evaluated their performance at four offshore locations. They found that bias at approximately 90 m ranged between  $-0.1 \text{ m s}^{-1}$  and  $+0.9 \text{ m s}^{-1}$ , depending on the location and model configuration. Thus, the large WRF bias at Humboldt exceeded the bias observed in these past studies and was unexpected in this study.

### 3.1 Short-Term Wind Speed Bias as a Function of Wind Speed

While the overall bias provides a general sense of model behavior over the short-term period of overlap with the lidar observations, it is helpful to understand how the bias varies as a function of observed wind speed. We calculated 120-m bias as a function of observed wind speed at both locations (Figure 4).

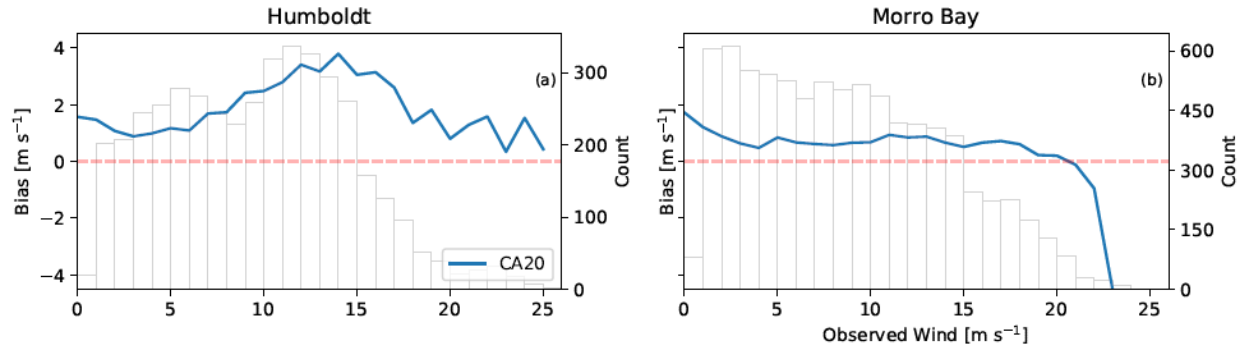


**Figure 4. The 120-m wind speed bias as a function of observed wind speed at (a) Humboldt and (b) Morro Bay. The number of hourly average observations in each wind speed bin (left y-axis) is overlaid as a bar plot.**

At Humboldt, we found the bias grew as observed wind speeds increased between about  $5 \text{ m s}^{-1}$  and  $14 \text{ m s}^{-1}$ , and the bias decreased beyond there. At Morro Bay, WRF had a bias below  $1 \text{ m s}^{-1}$  for observed winds between  $3 \text{ m s}^{-1}$  and  $21 \text{ m s}^{-1}$ . Beyond  $21 \text{ m s}^{-1}$ , WRF had a large negative bias, although there were very few observations ( $\sim 10\text{--}20$ ) in this range, so the statistics at this range are less conclusive.

### 3.2 Temporal Variability of Short-Term Wind Speed Bias

Next, we characterized how the observed bias varied with time of day and month of the year (Figure 5).

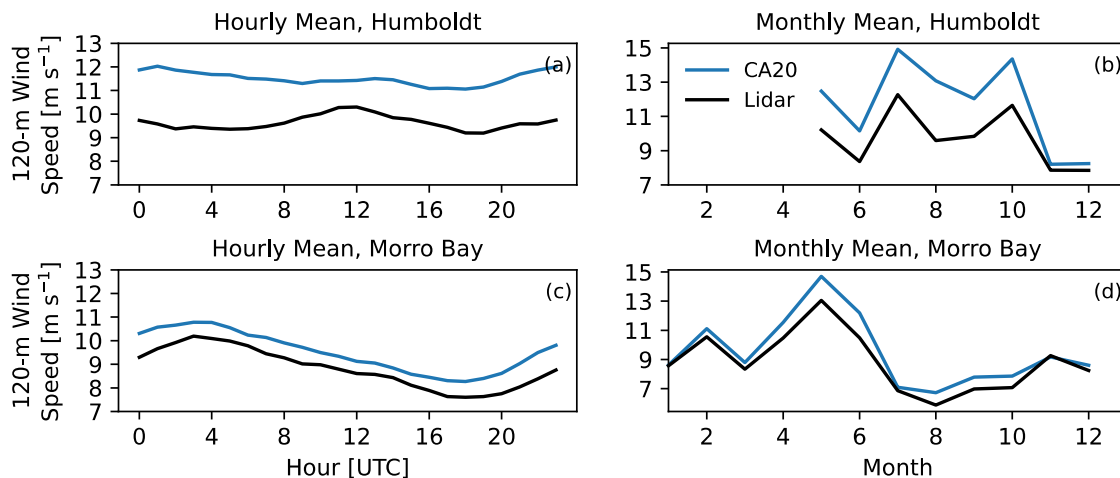


**Figure 5. The 120-m average wind speed as a function of hour at (a) Humboldt and (c) Morro Bay. Similarly, the 120-m average wind speed as a function of month at (b) Humboldt and (d) Morro Bay. Local time (Pacific Standard Time) may be found by subtracting 8 hours from the UTC time used in the plots.**

Observed winds at Humboldt had a small change in magnitude over the course of the average day, with a minimum wind speed of  $9.1 \text{ m s}^{-1}$  at 1800 UTC and a maximum of  $10.5 \text{ m s}^{-1}$  at 1100 UTC (note that Pacific Standard Time = UTC – 8 hours). WRF mischaracterized the timing of the wind speed diurnal cycle at Humboldt, with a larger bias between 2000 and 0400 UTC. On the other hand, at Morro Bay, the observed wind speed was strongest at 0300 UTC, and weakest near 1700 UTC. We found that WRF qualitatively captured the diurnal cycle at Morro Bay with a nearly constant bias throughout the average day.

As far as the annual cycle goes, we found that WRF tracked the variability of the observed monthly mean wind speeds. Observed winds at Morro Bay were stronger in spring than in fall and winter. Similarly, observed summertime winds at Humboldt were stronger than wintertime winds. At both locations, modeled mean monthly wind speeds increased and decreased at the same time as observed mean wind speeds, although the magnitude of the respective changes may disagree. At Humboldt, WRF bias was largest in August, during which it exceeded  $+4 \text{ m s}^{-1}$ .

The monthly analysis of winds can also help provide additional context on WRF’s large overall bias at Humboldt. At Humboldt, WRF’s wind speed bias was typically larger when wind speeds were larger. Lidar measurements are available at Humboldt during periods with the strongest winds, so it seems likely that WRF’s large overall bias would become smaller when gathering additional measurements from months with weaker winds. This aspect was further investigated in the long-term-adjusted validation; these results are described in Section 4.

### 3.3 Distributions of Wind Speed, Wind Direction, and Shear

While wind speed is the primary factor that dictates wind turbine power output, power output can also be substantially modified by shear and wind direction.

Wind shear is often characterized using the dimensionless wind shear exponent,  $\alpha$ , defined as:

$$\alpha = \frac{\ln \frac{WS_2}{WS_1}}{\ln \frac{z_2}{z_1}} \quad (1)$$

where  $z_1 = 40 \text{ m}$  and  $z_2 = 200 \text{ m}$  in all our calculations.

We compared observed and modeled distributions of wind speed, wind direction, and shear as shown in Figure 6.

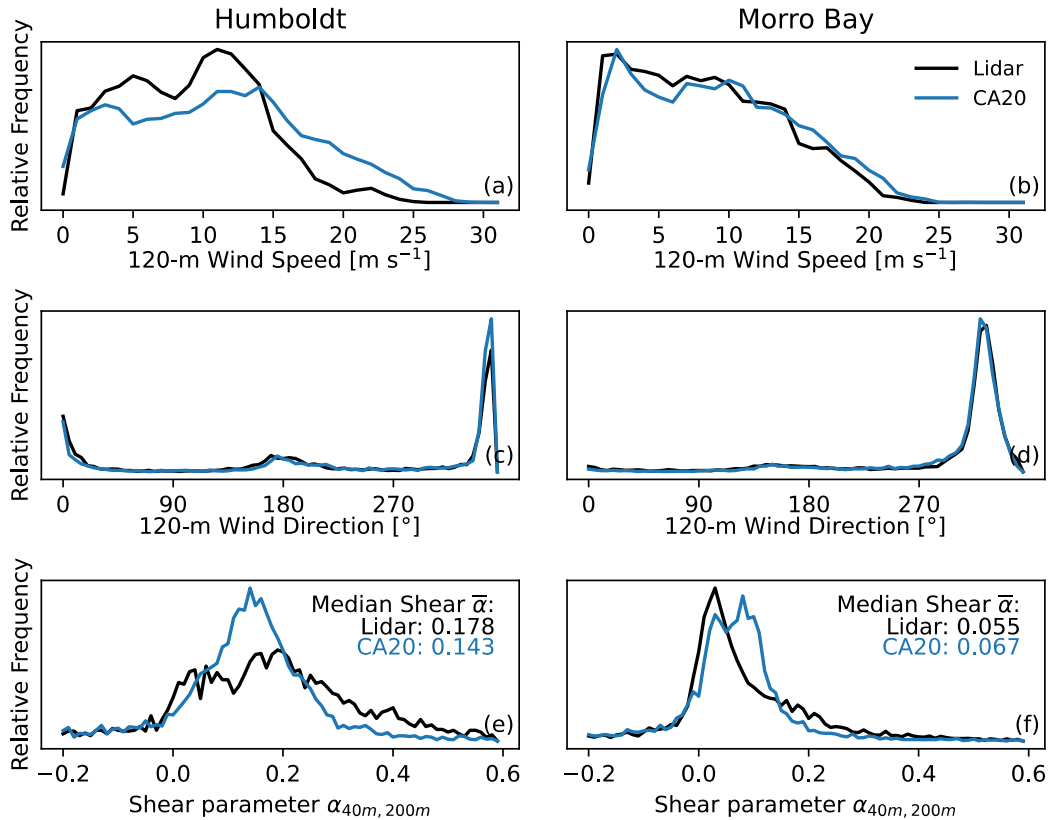


**Figure 6. Distributions of 120-m wind speed, 120-m wind direction, and the shear parameter calculated between 40 m and 200 m at (left) Humboldt and (right) Morro Bay**

We found that WRF overpredicts the frequency of winds stronger than  $15 \text{ m s}^{-1}$  and underpredicts the frequency of winds weaker than  $15 \text{ m s}^{-1}$  at Humboldt (Figure 6a). In contrast, the wind speed distributions from WRF and lidar observations agreed reasonably well at Morro Bay (Figure 6b). Despite the differences noted in wind speed distributions, modeled and observed 120-m wind direction distributions agreed well at both sites (Figures 6c, d). At Humboldt, winds were predominantly northerly, although some southerly winds occurred as well. At Morro Bay, winds were similarly predominantly north-northwesterly.

We found that the WRF model significantly deviated from the observed wind shear distribution at Humboldt, whereas at Morro Bay, the observed and modeled shear distributions were qualitatively more similar (Figures 6e, f). At Humboldt, WRF overpredicted the prevalence of moderate shear, and it underestimated the prevalence of stronger shear  $\alpha > 0.25$ . While WRF also underpredicted the prevalence of stronger shear at Morro Bay, its shear distribution shared a similar median with the observed distributions near  $\alpha = 0.05$ . Notably, the shape of the observed shear distributions at Humboldt and Morro Bay varied significantly. Morro Bay showed a higher prevalence of weaker shear (with a median shear of  $\alpha = 0.055$ ), whereas Humboldt more frequently showed stronger shear (with a median shear of  $\alpha = 0.178$ ).

## 4 Long-Term Validation Results

In general, validation metrics calculated over a short period of record will be different than those calculated over a long-term period. This fact is especially true if the shorter period of record is seasonally biased or characterized by anomalous conditions. Such conditions seemed to be the case for the Humboldt validation period, which was only 7 months in duration, lacked data for the period from January through April, and as is shown in Section 4.1, was characterized by highly anomalous wind speed conditions.

Because of these limitations, we also assessed the CA20 bias by evaluating the full 20-year modeled data set against a synthetic, long-term-corrected lidar data set over the same 20-year period, obtained by applying the MCP approach to the short-term lidar observations and the ERA-5 reanalysis product. Methods used for this validation and the subsequent results are presented in this section.

### 4.1 Lidar Period of Record Anomalies

First, we examined the mean 150-m wind speeds calculated from the 20-year CA20 data set at the two lidar locations, and compared that with the mean winds calculated from the 1-year extension of CA20. As shown in Table 2, mean winds at Humboldt were more than  $2 \text{ m s}^{-1}$  greater in the CA20 1-year extension than the original 20-year data set. By contrast, winds at Morro Bay were only  $0.6 \text{ m s}^{-1}$  greater in the 1-year extension.

**Table 2. Mean 150-m Wind Speeds From the 20-year CA20 and Its 1-Year Extension**

Site	Original CA20 Data Set (2000–2019) [ $\text{m s}^{-1}$ ]	CA20 Extended (Oct 2020–Sep 2021) [ $\text{m s}^{-1}$ ]
Humboldt	10.2	12.4
Morro Bay	9.1	9.7

To better understand these mean wind discrepancies, we considered distributions of monthly CA20 winds relative to those in the CA20 1-year extension. As shown in Figure 7, the 1-year extension of CA20 had highly anomalous winds in the July–October period—higher, in fact, than any monthly winds in the full 20-year period. By contrast, wind speeds at Morro Bay in the extended data set were more in line with the long-term distributions.

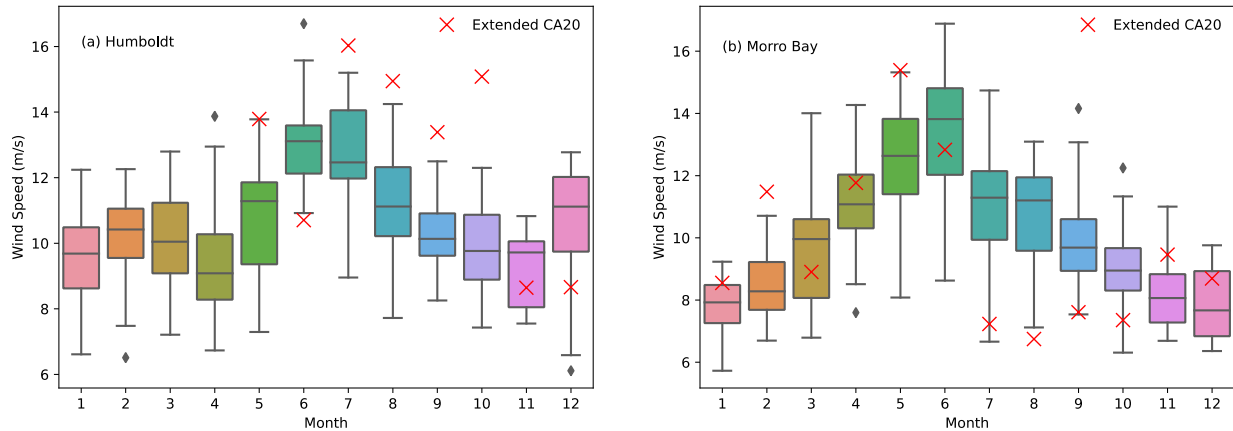


**Figure 7. Boxplots of the 20-year CA20 150-m monthly average wind speeds by calendar months at Humboldt (a) and Morro Bay (b). Black diamonds denote CA20 outliers. Red crosses denote the modeled mean monthly winds from the 1-year extension of CA20 over the lidar periods of record.**

## 4.2 A Long-Term Validation Approach

Because of the anomalies addressed in the previous section, it was likely that the bias found for the extended data set would differ from the original 20-year data set. To investigate the latter, we created a synthetic long-term-adjusted hourly lidar time series at both Humboldt and Morro Bay and, using these data as a benchmark, assessed the bias, cRMSE, and  $R^2$  in CA20.

To long-term correct the lidar data, we performed the following MCP steps:

1. Calculated hourly average 150-m<sup>1</sup> wind speeds from the original 10-minute lidar data.
2. Developed a second-order polynomial statistical fit between these hourly wind speeds and the concurrent hourly wind speed from the ERA5 100-m data product, extracted at the lidar locations.<sup>2</sup>
3. Used that fit to extend the lidar data sets to a long-term period covering the years 2000–2019.

Long-term adjustments were associated with uncertainty, which was inversely correlated with the length of the overlapping period of record between the two data sets as well as the correlation strength. As shown in Figure 8, we saw that correlation was reasonably strong between hourly lidar and ERA5 wind speeds. Furthermore, the large number of data points lended confidence to the ability to accurately long-term-adjust the lidar data.

<sup>1</sup> We used 150-m wind speeds since this was the hub height of the International Energy Agency Wind 15-MW power curve, which we considered in the next section.

<sup>2</sup> Ideally, 150-m winds from ERA5 would be used for a more robust regression relationship. However, only the 10-m and 100-m winds from ERA5 were made available directly for download, whereas winds at other heights required considerable effort in computation. For simplicity, we used the 100-m ERA5 winds here.

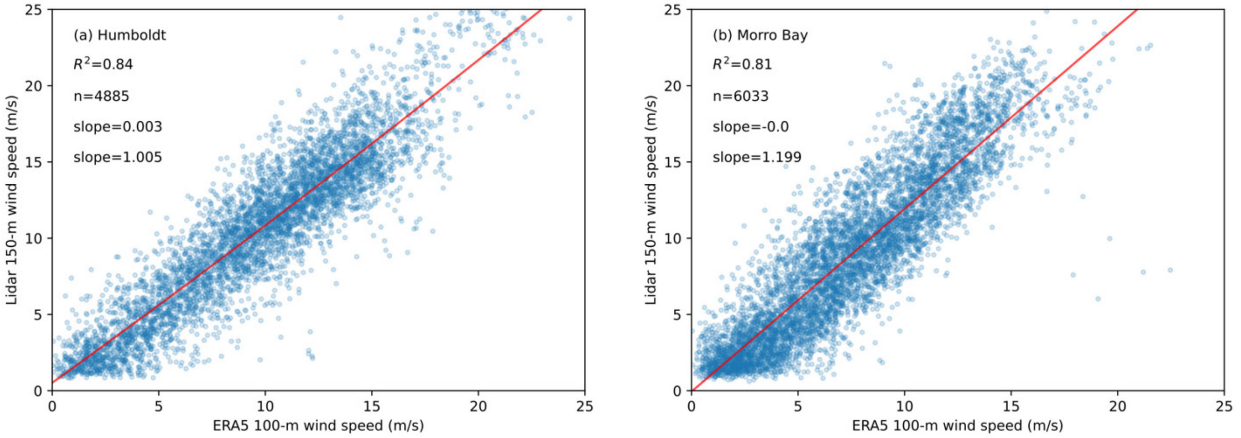


**Figure 8. Scatterplots of hourly 100-m ERA5 and 150-m lidar wind speeds at (a) Humboldt and (b) Morro Bay. The square of the correlation coefficient and number of data points are also shown.**

After applying the regression relationship to the ERA5 100-m wind speeds over the 2000–2019 period, we arrived at our synthetic, long-term-adjusted lidar time series data. A comparison of mean winds between this adjusted data set and CA20 is shown in Table 3. We saw the biases between sites were comparable and significantly lower than what we found in the short-term validation analysis.

**Table 3. Comparison of Mean 150-m Wind Speeds From Synthetic Long-Term-Corrected Lidar Data Set and CA20**

Site	Synthetic Long-Term-Adjusted Lidar Data Set (m s <sup>-1</sup> )	CA20 (m s <sup>-1</sup> )	CA20 Performance Metrics		
			Bias (m s <sup>-1</sup> )	cRMSE (m s <sup>-1</sup> )	R <sup>2</sup>
Humboldt	9.3	10.6	1.3	2.7	0.85
Morro Bay	9.0	10.0	1.0	2.8	0.78

### 4.3 Impact On Long-Term Energy

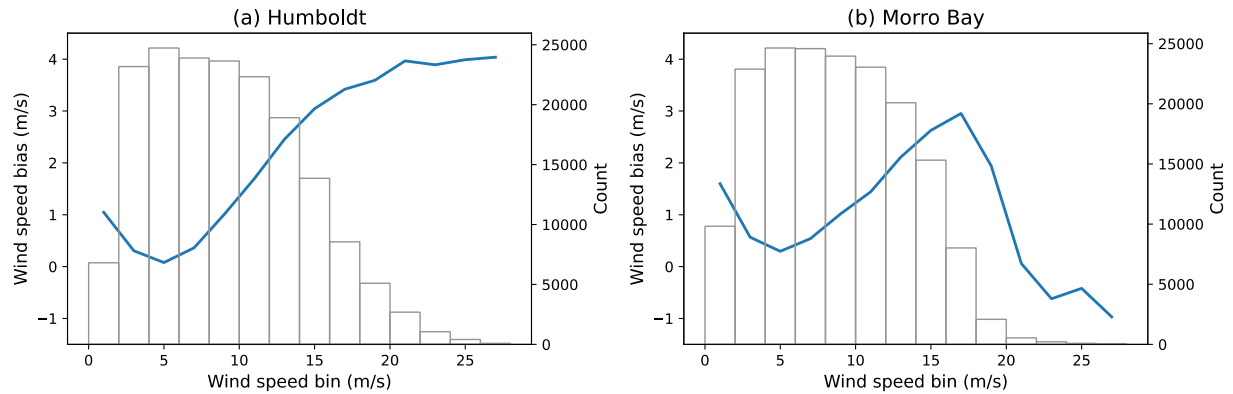
As a final exercise, we explored the impact that such wind speed bias would have on energy estimates for the Humboldt and Morro Bay wind energy areas. To do so, we took the hourly CA20 and synthetic long-term-adjusted lidar 150-m wind speed time series data, extracted at the lidar locations, and applied them to a single wind turbine using the International Energy Agency Wind 15-MW power curve. For simplicity, we made no air-density adjustments to the wind speeds. We present the average gross capacity factor (GCF) values in Table 4. Note that the CA20-derived values do not exactly match those given in Cooperman et al. (2022) due to the simplified approach implemented here.

Table 4 shows that, despite the high overall bias in mean winds, the impact on energy was less severe, with GCF decreases of 3.0 and 2.6 percentage points for Humboldt and Morro Bay, respectively, when synthetic long-term-adjusted lidar data were used in place of CA20 data.

**Table 4. Comparison of GCF Values Derived From the CA20 and Synthetic Long-Term-Adjusted Lidar Data Sets**

Site	GCF From Synthetic Long-Term-Adjusted Lidar Data Sets (%)	GCF from CA20 (%)	Difference (%)
Humboldt	55.6	58.6	3.0
Morro Bay	54.6	57.2	2.6

To understand this more modest impact on energy, Figure 9 shows where the CA20 wind speed bias actually occurred. Here, we plotted hourly bias in CA20 relative to the synthetic long-term-adjusted lidar for the 2000–2019 period and binned the results by wind speed. We saw that, especially for Humboldt, the highest bias occurred at high wind speeds (i.e., above 12 m s<sup>-1</sup>), where the International Energy Agency Wind 15-MW reference wind turbine was at rated capacity. In these conditions, a reduction in wind speed translated into a null change in produced energy, as long as the wind speed remained above the rated value. Also, we noted how winds rarely exceeded the 30 m s<sup>-1</sup> cut-out threshold at both sites.



**Figure 9. Mean biases of hourly CA20 150-m wind speeds relative to synthetic long-term-adjusted lidar 150-m wind speeds for (a) Humboldt and (b) Morro Bay. Data are binned based on hourly synthetic long-term lidar wind speeds. Data counts for each bin are also shown.**

## 5 Impact of the Choice of the Planetary Boundary Layer Scheme

Investigations on the reasons behind the mismatch between WRF simulation and lidar observations are currently underway. Preliminary results suggest that the choice of the PBL scheme in WRF might be connected to the large bias observed in CA20. Different PBL schemes adopt different assumptions connected to the transport of mass, moisture, and energy in the atmospheric boundary layer, which can cause differences in the model's representation of wind speed. To investigate this further, we ran a 1-year (October 2020–September 2021) WRF simulation using the same setup selected for CA20, but with a different PBL scheme—Yonsei University (YSU) instead of Mellor-Yamada-Nakanishi-Niino (MYNN). We then compared the WRF-simulated wind speed with the lidar observations, using the same process described for the main validation analysis. We found that the WRF simulation that adopted the YSU planetary boundary layer scheme had a significantly reduced bias, shown in Figure 10, both at Humboldt (+0.13 m s<sup>-1</sup>, averaged across all the considered heights) and Morro Bay (+0.03 m s<sup>-1</sup>, averaged across all the considered heights). The YSU Weather Research and Forecasting setup also reduced the cRMSE, especially at Humboldt, whereas the R<sup>2</sup> coefficient did not seem to be strongly impacted by the choice of the PBL scheme.

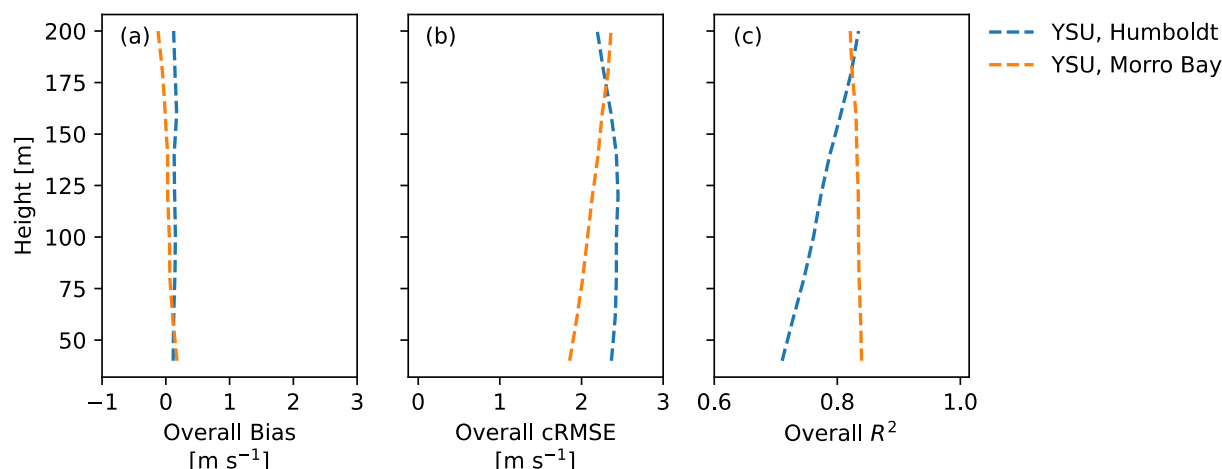


**Figure 10. (a) Bias, (b) cRMSE, and (c) R<sup>2</sup> calculated at Humboldt and Morro Bay for the WRF validation run using the YSU planetary boundary layer scheme, compared to the floating lidar observations**

Figure 11 compares the distributions of modeled and observed 120-m wind speed, wind direction, and shear coefficient (between 40 m and 200 m). The updated WRF simulation provided a closer match with the lidar observations both in terms of the wind speed and wind shear distributions, which were not accurately captured by the original CA20 setup. The modeled wind direction distributions remained accurate, as already observed for the original CA20 setup in Figure 6.

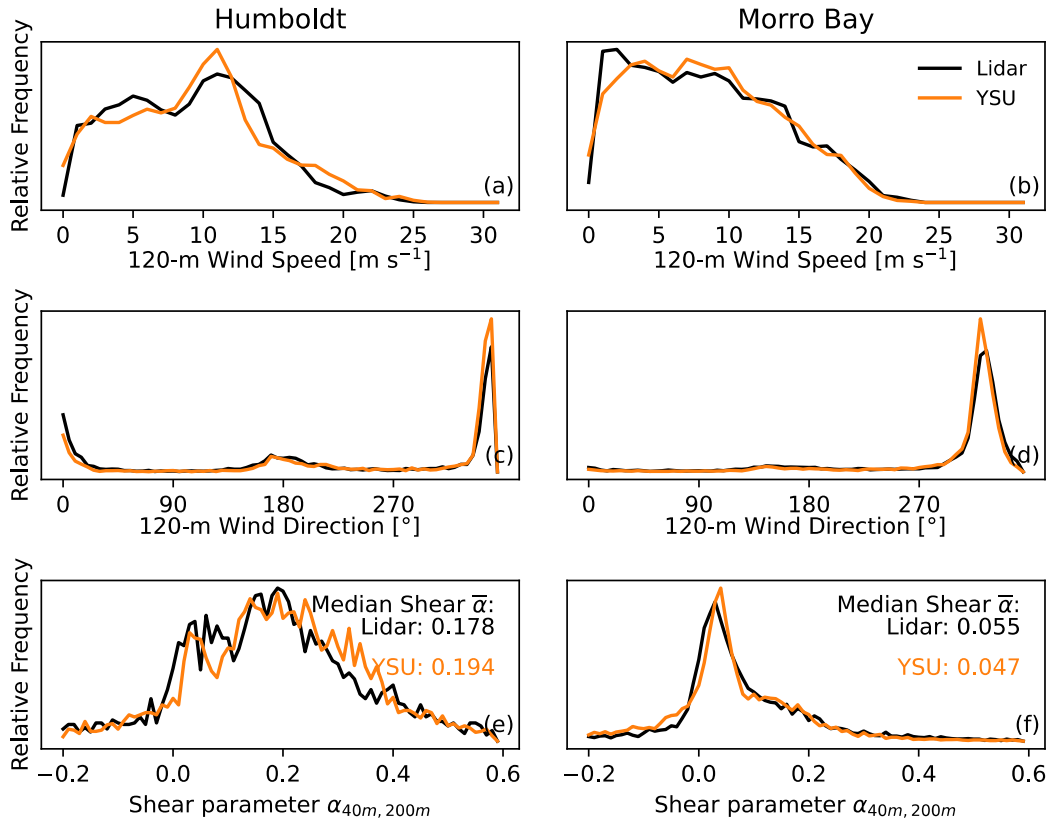


**Figure 11. Distributions of 120-m wind speed, 120-m wind direction, and the shear parameter calculated between 40 m and 200 m at (left) Humboldt and (right) Morro Bay. Results shown in the figure are for the WRF simulation that uses the YSU PBL scheme.**

Preliminary results from a PNNL case study analysis showed that the large difference between the wind speed modeled by the MYNN and YSU setups was associated with stronger vertical turbulent mixing aloft in the MYNN setup, which had the effect of entraining high momentum from a topography and thermally induced, persistent low-level jet downward to hub height. By contrast, the YSU setup estimated less mixing aloft, modeled less entrainment, and thus predicted lower wind speeds at hub height. Results of PNNL’s investigative work will be summarized in a report in early 2023.

## 6 Conclusions and Next Steps

The analysis completed to date has shown high bias in the CA20 modeled wind resource data set, relative to floating lidar observations in offshore California wind energy areas. However, the impact on energy estimates is less severe because most of the bias occurred at high wind speed regimes when wind turbines would already be operating at rated power. Overall, long-term gross capacity factor estimates are about 3 percentage points higher when using only the CA20 wind resource data, compared to using a synthetic, long-term-adjusted lidar wind speed data set obtained by applying the MCP method to the short-term lidar observations and the ERA-5 reanalysis product.

While the available lidar observations provide a way to quantify and account for the model bias found at the Humboldt and Morro Bay lease areas, quantifying and accounting for potential model bias at other wind energy areas that lack lidar measurements (e.g., the Cape Mendocino wind energy area) will be more problematic. For this reason, further understanding and characterizing the bias are crucial. To this end, NREL and PNNL are continuing to investigate the physical drivers of bias in the CA20 data.

Over the next few months, NREL and PNNL will further investigate and characterize the bias by:

- **Confirming the low-level jet momentum entrainment mechanism over a full calendar year.** PNNL's promising results were based on several case studies totaling less than 10 days of simulation. NREL will use the extended CA20 data sets to confirm the presence of a persistent low-level jet in California and higher momentum entrainment in MYNN over a full calendar year.
- **Re-running CA20 using the YSU setup.** Given the strong performance of the YSU-based runs, NREL will reproduce a 20-year CA20 data set using this setup. This new data set will replace the original CA20.
- **Validating the new CA20 setup.** Once the new 20-year YSU-based CA20 data set is complete, NREL will extensively validate the new data set using a network of buoy measurements and coastal radar data over the full 2000–2019 period.
- **Assessing the potential bias of NREL's 20-year wind resource data sets for Hawaii and the Pacific Northwest.** Both data sets were run with the same MYNN parameterization as CA20. To address the potential bias of these data sets, and without any lidar data, NREL will run 1-year simulations of the YSU setup for each region and compare modeled wind speeds to the original MYNN runs.

## References

Atmosphere to Electrons. 2021. Lidar - California - Leosphere Windcube 866 (130), Morro Bay - Processed Data. Maintained by A2e Data Archive and Portal for U.S. Department of Energy, Office of Energy Efficiency and Renewable Energy. DOI: 10.21947/1783809.

<https://a2e.energy.gov/ds/buoy/lidar.z06.a0> Accessed: June 1, 2022.

Atmosphere to Electrons. 2022. Lidar - California - Leosphere Windcube 866 (120), Humboldt - Processed Data. Maintained by A2e Data Archive and Portal for U.S. Department of Energy, Office of Energy Efficiency and Renewable Energy. DOI: 10.21947/1783809.

<https://a2e.energy.gov/ds/buoy/lidar.z05.a0> Accessed: June 1, 2022.

Brower, M. 2012. *Wind Resource Assessment: A Practical Guide to Developing a Wind Project*. John Wiley & Sons, Hoboken, New Jersey, USA. <https://doi.org/10.1002/9781118249864>.

Cooperman, A., P. Duffy, M. Hall, E. Lozon, M. Shields, and W. Musial. 2022. *Assessment of Offshore Wind Energy Leasing Areas for Humboldt and Morro Bay Wind Energy Areas, California*. Golden, CO: National Renewable Energy Laboratory. NREL/TP-5000-82341.

<https://www.nrel.gov/docs/fy22osti/82341.pdf>.

Hahmann, A. N., T. Sīle, B. Witha, N. N. Davis, M. Dörenkämper, Y. Ezber, E. García-Bustamante, J. F. González-Rouco, J. Navarro, B. T. Olsen, and S. Söderberg. 2020. “The making of the New European Wind Atlas – Part 1: Model sensitivity.” *Geosci. Model Dev.*, 13, 5053–5078. <https://doi.org/10.5194/gmd-13-5053-2020>.

Hersbach, H., B. Bell, P. Berrisford, S. Hirahara, A. Horányi, J. Muñoz-Sabater, J. Nicolas, C. Peubey, R. Radu, D. Schepers, et al. 2020. “The ERA5 global reanalysis.” *Quarterly Journal of the Royal Meteorological Society*, 146, no. 730: 1999–2049. <https://doi.org/10.1002/qj.3803>.

Optis, M., A. Rybchuk, N. Bodini, M. Rossol, and W. Musial. 2020. *2020 Offshore Wind Resource Assessment for the California Pacific Outer Continental Shelf*. Golden, CO: National Renewable Energy Laboratory. NREL/TP-5000-77642.

<https://www.nrel.gov/docs/fy21osti/77642.pdf>.

Pronk, V., N. Bodini, M. Optis, J. K. Lundquist, P. Moriarty, C. Draxl, A. Purkayastha, and E. Young. 2022. “Can reanalysis products outperform mesoscale numerical weather prediction models in modeling the wind resource in simple terrain?” *Wind Energ. Sci.*, 7, 487–504.

<https://doi.org/10.5194/wes-7-487-2022>.